University of Thi-Qar Journal of Science (UTJsci)
E-ISSN: 2709-0256, P-ISSN: 1991-8690, Vol. 11, No. 1, Jun. 2024

Susceptibility in a Coupled Double Quantum Dot-Metal Nanoparticle System under Standing Wave Field

Haneen Akram *[1a], Muwaffaq Abdullah [1b], El Mustapha Feddi [2c] , Amin H. Al-Khursan [1d] and Ali M. Muslim [3e]

[1]*Nasiriya Nanotechnology Research Laboratory (NNRL), College of Science,University of Thi-Qar Nasiriya, Iraq*
[2]*Group of Optoelectronic of Semiconductors and Nanomaterials, ENSAM, Mohammed V University in Rabat, Morocco.*
[3]*Department of Computer and Communication System Engineering, Universiti Putra Malaysia, Serdang, Malaysia*

[b]E-mail: mowaffaq_2phy@sci.utq.edu.iq, [c] E-mail: e.feddi@um5r.ac.ma,
[d]E-mail: ameen_2all@yahoo.com, [e] E-mail: gs52755@pelajar.upm.edu.my.
[a]**E-mail:* haneen_akr.ph@sci.utq.edu.iq.

Received: 2023-12-30, Revised: 2024-01-24, Accepted: 2024-01-31, Published: 2024-06-01

***Abstract*— The main purpose of this work is studying the linear Susceptibility in the hybrid nanostructure that composed of a dual quantum dot (DQD) and metal nanoparticle (MNP) hybrid system under a standing-wave field. In our model, we used density matrix equations by taking into our account the interaction between excitons and surface plasmons. The proposed DQD is composed of two QDs. Each QD contains an InAs QD with a disk shape. The interaction between the QD and the wetting layer (WL) is taken into consideration. The application of the standing wave field on DQD-MNP hybrid system was modeled and examined. The susceptibility of thehybridDQD-MNPsystem reduced by the pump field under a standing-wave field. The high susceptibility obtained with a wide MNP radius. An interesting result was shown in the inversion of the grating period with the tunneling component in the conduction band. The smaller size of DQD gave us high susceptibility due to the quantization effect.**

***Keywords*—Double quantum dot, metal nanoparticle, Standing-Wave, Susceptibility**

I. INTRODUCTION

When metallic nanostructures and semiconductor quantum dots (QDs) are adjacent to each other, an interaction between QD exciton states and metal surface plasmons occurs. Thus, it modifies the electromagnetic field experienced by quantum systems. Additionally, the optical properties of Nano systems like QDs with plasmonic nanoparticles, metallic nanorods and spherical nanoparticles, have recently attracted a lot of attention [1-4].

In recent years, there has been a rapid progression in nanostructure techniques, particularly in the domains of magnetic nanoparticles (MNPs) and quantum dots (QDs), contributing to increased affordability. Studying these nanostructures is crucial for understanding their characteristics better. It's an interesting subject to study various optical processing devices. Recent rresearch has examined several exciting occurrences in hybrid nanostructure made up of MNPs and QDs, like energy transfer [5], local domain enhancement [6], thermal effects [7], tunable ultrafast Nano-switches [8], modified resonance-fluorescence, photon statistics [9], controlled slow light [10], second-harmonic generation [11], gain without inversion [12,13], intrinsic optical biostability [14,15], creation of difference-frequency generation [16], and third-order wave-mixing processes [17-21]. Due to the exciton's interaction with surface plasmons, a coupled MNP-QD system interacting with a strong pump field and a weak probe field produces unusual optical characteristics, especially in the dispersion and absorption spectra [22-26]. Sadeghi suggested using the QD-MNP distance to control an adjustable gain without inversion. More specifically, a plasmonic resonance and an extremely high gain without inversion were obtained at a crucial distance between MNP and QD [20, 23].

The linear susceptibility of DQD-MNP hybrid system standing-wave field was analyzed and computed in this work. The hybrid complex consists of a small DQD and a spherical MNP that interact with both fields a strong pump and a weak probe. DQD system was proposed considering both valence (VB), conduction bands (CB), and WL. This was explained by the updated density matrix equations including the surface plasmon-exciton interaction.

II. MODEL AND THEORY

A. *The DQD- MNP system*

The hybrid structure that was demonstrated in this research is composed of spherical MNP of radius a and dielectric function ε_M and a DQDofradii ρ_1, ρ_2. The DQD's dielectric constant is ε_s. The dielectric constant of the medium in which the whole system is embedded is ε_B, as illustrated in Figure 1. The distance between particles was represented by R and appeared to be longer than the MNP's radius ($R > a > \rho_1, \rho_2$) [14,17] where ρ_i relates to any one of the two QDs' radius.

A gold (Au) sphere is the MNP that was frequently utilized in the references [1, 3-8,17]. DQD is made up of two QDs, an InAs with a height of h_d and a radius of ρ on a disk shape. The height of the first QD was $h_d = 0.1\text{nm}$ and its radius was $\rho_1 = 3\text{nm}$. The second QD was with height of

https://doi.org/10.32792/utq/utjsci/v11i1.1156

h_d = 0.15 nm, and radius of $\rho_2 = 4$nm. Every QD has a single conduction and valence subband. DQD that was grown on a WL with 10-nm-thick InGaAs quantum well layer.

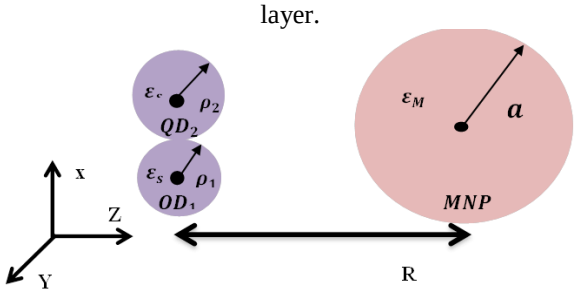

Figure 1: A DQD of radius ρ connected to an MNP of radius a makes up the hybrid system.

B. The Hamiltonian

The hybrid structure comprising double quantum dots (DQD) and magnetic nanoparticles (MNP) exhibits interactions with both probe and pump fields. Considering that the probe field formula is $(\mathrm{E}_{02}(\mathrm{t}) = \frac{E_{02}^0}{2} e^{-i\omega_{02}t} + \mathrm{c.c.})$ with an amplitude(E_{02}^0) between $(|0\rangle \leftrightarrow |2\rangle)$ and frequency (ω_{02}) . In the same way, a pump laser field $(\mathrm{E}_{13}(\mathrm{t}) = \frac{E_{13}^0}{2} e^{-i\omega_{13}t} + \mathrm{c.c.})$ with amplitude (E_{13}^0) was applied between states $(|1\rangle \leftrightarrow |3\rangle)$ and frequency (ω_{13}).

Using density matrix theory, the dynamics of the DQD system are described by the following equation of motion [27],

$$\dot{\rho_{ij}} = \frac{-i}{\hbar}[H, \rho_{ij}] \quad (1)$$

The system's Hamiltonian can be expressed following the discussion of the QD-MNP hybrid system in previous works [16, 28, 29],

$$H = \mathrm{H}_0 + \mathrm{H}_{int} + \mathrm{H}_{relax} \quad (2)$$

Where is H_0 the unperturbed Hamiltonian, $\mathrm{H}_0 = \sum_{i=0}^{5} \hbar\omega_i$, H_{relax} is the relaxation Hamiltonian. In this work, H_{int} represents the interaction between was expressed as

$$H_{int} = \begin{bmatrix} 0 & T_{01} & \Omega_{20} & \beta_{30} & \beta_{40} & 0 \\ T_{01} & 0 & \beta_{21} & \Omega_{31} & \beta_{41} & 0 \\ \Omega_{20} & \beta_{21} & 0 & T_{32} & 0 & \beta_{52} \\ \beta_{30} & \Omega_{31} & T_{32} & 0 & 0 & \beta_{53} \\ \beta_{40} & \beta_{41} & 0 & 0 & 0 & \beta_{54} \\ 0 & 0 & \beta_{52} & \beta_{53} & \beta_{54} & 0 \end{bmatrix}$$

$$+ \begin{bmatrix} 0 & 0 & \mathrm{G}_{20} & 0 & 0 & 0 \\ 0 & 0 & 0 & \mathrm{G}_{31} & 0 & 0 \\ \mathrm{G}_{20} & 0 & 0 & 0 & 0 & 0 \\ 0 & \mathrm{G}_{31} & 0 & 0 & 0 & 0 \\ 0 & 0 & 0 & 0 & 0 & 0 \\ 0 & 0 & 0 & 0 & 0 & 0 \end{bmatrix} [\rho_{ij}] \quad (3)$$

Where T_{01} and T_{32} represent the tunneling components, $\beta_{ij} = \frac{\mathrm{A_{ij}}}{2} + \frac{1}{\tau_t}$, with $\mathrm{A_{ij}}(= \frac{{\mu_{ij}}^2 \omega_{ij}^2}{3\pi\hbar\varepsilon_s c^3})$ is the Einstein coefficient, G_{ij} is the DQD's self-interaction, ρ_{ij} is DQD density matrix operator.

C. The DQD- MNP fields

There are two components of the DQD systems inside electric field $(\mathrm{E_{DQD,ij}})$. The fields were generated by the polarization of the MNP and those applied externally. It was approximated quasi-statically by [28],

$$\mathrm{E_{DQD,ij}} = \frac{\mathrm{E_{ij}}}{\varepsilon_{\mathrm{effs}}} + \frac{\delta_\alpha \mathrm{P_{MNP,ij}}}{4\pi\varepsilon_\mathrm{B}\varepsilon_{\mathrm{effs}}\mathrm{R}^3} \quad (4)$$

$\mathrm{E_{ij}}$ refers to any of the applied fields (probe E_{02} or pump E_{13}), $\varepsilon_{\mathrm{effs}} = \frac{2\varepsilon_\mathrm{B}+\varepsilon_\mathrm{s}}{3\varepsilon_\mathrm{B}}$, ε_B is the environment dielectric constant, and $\delta_\alpha = 2$. The interparticle axis (Z-axis) and the applied fields are parallel. MNP's surface-induced charge, which causes its polarization, was expressed as,

$$\mathrm{P_{MNP,ij}} = 4\pi\varepsilon_\mathrm{B}\gamma_\mathrm{M}\mathrm{a}^3\mathrm{E_{ij}} + \frac{\gamma_\mathrm{M}\mathrm{a}^3\delta_\alpha \mathrm{P_{DQD,ij}}}{\varepsilon_{\mathrm{effs}}\mathrm{R}^3} \quad (5)$$

$\gamma_\mathrm{M} = (\frac{\varepsilon_\mathrm{M}(\omega)-\varepsilon_\mathrm{B}}{2\varepsilon_\mathrm{B}+\varepsilon_\mathrm{M}(\omega)})$, while the DQD polarization is [30],

$$\mathrm{P_{DQD,ij}} = \mu_{\mathrm{ij}}\left(\rho_{\mathrm{ij}}\mathrm{e}^{-\mathrm{i}\omega_{\mathrm{ij}}\mathrm{t}} + \rho_{\mathrm{ij}}\mathrm{e}^{\mathrm{i}\omega_{\mathrm{ji}}\mathrm{t}}\right) \quad (6)$$

Then,

$$\mathrm{P_{MNP,ij}} = \left(\frac{4\pi\varepsilon_\mathrm{B}\mathrm{a}^3\gamma_\mathrm{M}\mathrm{E_{ij}^0}}{2} + \frac{\mathrm{a}^3\gamma_\mathrm{M}\delta_\alpha\mu_{\mathrm{ij}}}{\varepsilon_{\mathrm{effs}}\mathrm{R}^3}\rho_{\mathrm{ij}}\right)\mathrm{e}^{-\mathrm{i}\omega_{\mathrm{ij}}\mathrm{t}} + \left(\frac{4\pi\varepsilon_\mathrm{B}\mathrm{a}^3\gamma_\mathrm{M}\mathrm{E_{ij}^0}}{2} + \frac{\mathrm{a}^3\gamma_\mathrm{M}\delta_\alpha\mu_{\mathrm{ji}}}{\varepsilon_{\mathrm{effs}}\mathrm{R}^3}\rho_{\mathrm{ji}}\right)\mathrm{e}^{\mathrm{i}\omega_{\mathrm{ji}}\mathrm{t}} \quad (7)$$

The applied field's amplitude was expressed as $\mathrm{E_{ij}^0}$, while the transition momentum was represented by μ_{ij}. Using the results of Eqs. (4)–(7),

$$\mathrm{E_{DQD,ij}} = \frac{\hbar}{\mu_{\mathrm{ij}}}\left[(\Omega_{\mathrm{ij}} + \mathrm{G_{ij}}\rho_{\mathrm{ij}})\mathrm{e}^{-\mathrm{i}\omega_{\mathrm{ij}}\mathrm{t}} + (\Omega_{\mathrm{ji}}^* + \mathrm{G_{ji}^*}\rho_{\mathrm{ji}})\mathrm{e}^{\mathrm{i}\omega_{\mathrm{ji}}\mathrm{t}}\right] \quad (8)$$

where Ω_{ij} represents the effective Rabi frequency of the pump Ω_{13} field or the probe Ω_{02} field, respectively, and it is expressed as:

$$\Omega_{\mathrm{ij}} = \Omega_{\mathrm{ij}}^0\left(1 + \frac{\gamma_\mathrm{M}\mathrm{a}^3\delta_\alpha}{\mathrm{R}^3}\right) \quad (9)$$

The direct coupling of DQD was indicated by the first term of the Rabi frequency $\Omega_{\mathrm{ij}}^0(= \frac{\mathrm{E_{ij}^0}\mu_{\mathrm{ij}}}{2\hbar\varepsilon_{\mathrm{effs}}})$ the second term represents the field that was generated by the MNP as a result of its interaction with the applied field. The parameter $\mathrm{G_{ij}}$ represents the self-interaction of the DQD [15]:

$$\mathrm{G_{ij}} = \frac{\gamma_\mathrm{M}\mathrm{a}^3}{4\pi\varepsilon_\mathrm{B}\hbar\mathrm{R}^6}(\frac{\mu_{\mathrm{ij}}\delta_\alpha}{\varepsilon_{\mathrm{effs}}})^2 \quad (10)$$

Where the DQD and MNP are polarized by the applied field that was generated by the interacting with the DQD to produce$\mathrm{G_{ij}}$ [29].

D. Density matrix equations of the DQD-MNP system

DQD-MNP system's band energy diagram is shown in Figure 2. DQD system has two states. One state is in the CB, $|0\rangle$ and $|1\rangle$, and the second state is in the VB, $|2\rangle$ and $|3\rangle$. WL CB state was represented by state $|4\rangle$, and the WL VB state was represented by state $|5\rangle$. However, our results were different from what has been mentioned in the literature [31-33]. With DQD states, MNP energies are shown as a quasi-continuum state. Additionally, Rabi

frequencies Ω_{ij}^{0}, the tunneling components T_{01} and T_{32} are shown in the DQD system

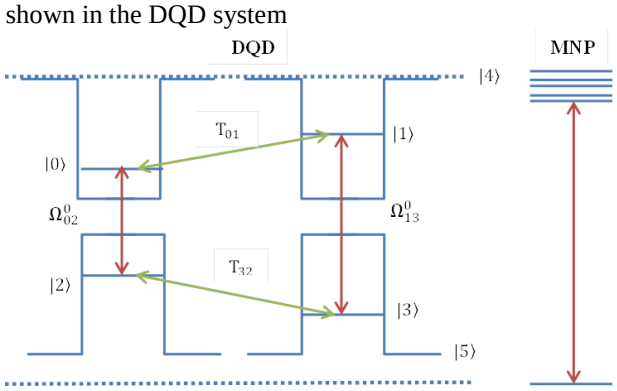

Fig. 2. Diagram of DQD - MNP system's energy band withWL.

$$\dot{\rho_{00}} = -\gamma_0\rho_{00} + i[T_{01}(\rho_{10} - \rho_{01}) + (\Omega_{20} + G_{20}\rho_{20})(\rho_{20} - \rho_{02}) + \beta_{30}(\rho_{30} - \rho_{03}) + \beta_{40}(\rho_{40} - \rho_{04})]$$

$$\dot{\rho_{11}} = -\gamma_1\rho_{11} + i[T_{01}(\rho_{01} - \rho_{10}) + \beta_{21}(\rho_{21} - \rho_{12}) + (\Omega_{31} + G_{31}\rho_{31})(\rho_{31} - \rho_{13}) + \beta_{41}(\rho_{41} - \rho_{14})]$$

$$\dot{\rho_{22}} = -\gamma_2\rho_{22} + i[(\Omega_{20} + G_{20}\rho_{20})(\rho_{02} - \rho_{20}) + \beta_{21}(\rho_{12} - \rho_{21}) + T_{32}(\rho_{32} - \rho_{23}) + \beta_{52}(\rho_{25} - \rho_{52})]$$

$$\dot{\rho_{33}} = -\gamma_3\rho_{33} + i[\beta_{30}(\rho_{03} - \rho_{30}) + (\Omega_{31} + G_{31}\rho_{31})(\rho_{13} - \rho_{31}) + T_{32}(\rho_{23} - \rho_{32}) + \beta_{53}(\rho_{35} - \rho_{53})]$$

$$\dot{\rho_{44}} = -\gamma_4\rho_{44} + i[\beta_{40}(\rho_{04} - \rho_{40}) + \beta_{41}(\rho_{14} - \rho_{41})]$$

$$\dot{\rho_{55}} = -\gamma_5\rho_{55} + i[\beta_{52}(\rho_{52} - \rho_{25}) + \beta_{53}(\rho_{53} - \rho_{35}) + \beta_{54}(\rho_{54} - \rho_{45})]$$

$$\dot{\rho_{10}} = -(\gamma_0+\gamma_1)\rho_{10} + i[T_{01}(\rho_{00} - \rho_{11}) + \beta_{21}\rho_{20} + (\Omega_{31} + G_{31}\rho_{31})\rho_{30} + \beta_{41}\rho_{40} - (\Omega_{20} + G_{20}\rho_{20})\rho_{12}]$$

$$\dot{\rho_{20}} = [-(\gamma_0+\gamma_2) - i\Delta_{20}]\rho_{20} + i[(\Omega_{20} + G_{20}\rho_{20})(\rho_{00} - \rho_{22}) + \beta_{21}\rho_{10} + T_{32}\rho_{30} + \beta_{30}\rho_{23} + \beta_{52}\rho_{50} - T_{01}\rho_{21} - \beta_{40}\rho_{24}]$$

$$\dot{\rho_{30}} = -(\gamma_0+\gamma_3)\rho_{30} + i[\beta_{30}(\rho_{00} - \rho_{33}) + (\Omega_{31} + G_{31}\rho_{31})\rho_{10} + T_{32}\rho_{20} - T_{01}\rho_{31} - (\Omega_{20}\ vdss + G_{20}\rho_{20})\rho_{32} - \beta_{40}\rho_{34}]$$

$$\dot{\rho_{40}} = -(\gamma_0+\gamma_4)\rho_{40} + i[\beta_{40}(\rho_{00} - \rho_{44}) - \beta_{41}\rho_{10} - (\Omega_{20} + G_{20}\rho_{20})\rho_{42} - \beta_{30}\rho_{43} - T_{01}\rho_{41} + \beta_{40}\rho_{34}]$$

$$\dot{\rho_{50}} = -(\gamma_0+\gamma_5)\rho_{50} + i[\beta_{52}\rho_{20} + \beta_{53}\rho_{30} + \beta_{54}\rho_{40} + (\Omega_{20} + G_{20}\rho_{20})\rho_{52} - \beta_{30}\rho_{53} - \beta_{40}\rho_{54}]$$

$$\dot{\rho_{21}} = -(\gamma_1+\gamma_2)\rho_{21} + i[\beta_{21}(\rho_{11} - \rho_{22}) - (\Omega_{20} + G_{20}\rho_{20})\rho_{01} - T_{10}\rho_{20} + T_{32}\rho_{31} - (\Omega_{31} + G_{31}\rho_{31})\rho_{23} - \beta_{41}\rho_{24} + \beta_{25}\rho_{51}]$$

$$\dot{\rho_{23}} = -(\gamma_2+\gamma_3)\rho_{23} + i[T_{32}(\rho_{33} - \rho_{22}) + (\Omega_{20} + G_{20}\rho_{20})\rho_{03} - \beta_{03}\rho_{20} + \beta_{21}\rho_{13} - (\Omega_{31} + G_{31}\rho_{31})\rho_{21} + \beta_{25}\rho_{53} - \beta_{53}\rho_{25}]$$

$$\dot{\rho_{24}} = -(\gamma_2+\gamma_4)\rho_{24} + i[(\Omega_{20} + G_{20}\rho_{20})\rho_{04} - \beta_{04}\rho_{20} + \beta_{21}\rho_{14} - \beta_{14}\rho_{21} + T_{32}\rho_{34} + +\beta_{25}\rho_{54} - \beta_{54}\rho_{25}]$$

$$\dot{\rho_{25}} = -(\gamma_2+\gamma_5)\rho_{25} + i[\beta_{25}(\rho_{55} - \rho_{22}) + (\Omega_{20} + G_{20}\rho_{20})\rho_{05} + \beta_{21}\rho_{15} + T_{32}\rho_{35} - \beta_{35}\rho_{23} + \beta_{24}\rho_{45} - \beta_{45}\rho_{24} + \beta_{25}\rho_{55}]$$

$$\dot{\rho_{31}} = -(\gamma_1+\gamma_3)\rho_{31} + i[(\Omega_{31} + G_{31}\rho_{31})(\rho_{11} - \rho_{33}) + \beta_{30}\rho_{01} - T_{01}\rho_{30} + \beta_{21}\rho_{32} + T_{32}\rho_{21} - \beta_{35}\rho_{51} - \beta_{41}\rho_{34}]$$

$$\dot{\rho_{41}} = -(\gamma_1+\gamma_4)\rho_{41} + i[\beta_{41}(\rho_{11} - \rho_{44}) + \beta_{40}\rho_{01} - T_{01}\rho_{40} - \beta_{21}\rho_{42} + \beta_{45}\rho_{51} - (\Omega_{31} + G_{31}\rho_{31})\rho_{43}]$$

$$\dot{\rho_{34}} = -(\gamma_3+\gamma_4)\rho_{34} + i[\beta_{40}\rho_{03} + \beta_{41}\rho_{13} - \beta_{03}\rho_{40} + (\Omega_{31} + G_{31}\rho_{31})\rho_{41} - T_{32}\rho_{42}]$$

$$\dot{\rho_{35}} = -(\gamma_3+\gamma_5)\rho_{35} + i[\beta_{30}\rho_{05} + T_{32}\rho_{25} - \beta_{25}\rho_{32} + \beta_{35}\rho_{55} + (\Omega_{31} + G_{31}\rho_{31})\rho_{15} + \beta_{35}(\rho_{55} - \rho_{33})]$$

$$\dot{\rho_{51}} = -(\gamma_1+\gamma_5)\rho_{51} + i[\beta_{52}\rho_{21} - T_{01}\rho_{50} - (\Omega_{31} + G_{31}\rho_{31})\rho_{53} + \beta_{53}\rho_{31} - \beta_{21}\rho_{52} + \beta_{54}\rho_{41} - \beta_{41}\rho_{41}] \quad (11)$$

With the condition,

$$\rho_{00} + \rho_{11} + \rho_{22} + \rho_{33} = 1$$

where ω_2 represents the resonant frequency of the second QD2 state, Δ_{20} is detuning with $\Delta_{20} = \omega_2 - \omega_{02}$, and γ_i is relaxation rate. Density operators ρ_{44}, ρ_{55} are for WL occupations and $\rho_{i4}, \rho_{4j}, \rho_{i5}, \rho_{5j}$ for WL interactions.

E. Momentum matrix elements

One important aspect of this study was to compute the momentum matrix element μ_{ij} of each interdot transition, as well as the calculation of each momentum matrix element μ_{iw} of each WL-QD transition. Calculating momenta is necessary due to its crucial function in determining optical property parameters, especially Rabi frequencies found in Equations (8), (9), and (10), besides its implicit function in the computation of G_{ij} and Ω_{ij} which they present within the density matrix equations:[34],

$$\mu_{12} = C_{mn}\left\{\int_0^a J_m(p_1\rho)J_m(p_2\rho)e\rho^2 d\rho\right\}$$

$$\left\{\int_0^{h_d}\left[\cos(k_{z_1}z)\cos(k_{z_2}z)\right]\right\}dz\int_0^{2\pi}\frac{1}{2\pi}d\phi \quad (12)$$

In this case, the normalization constant is C_{mn}, e is the electronic charge. The QD state |i⟩ in the z-direction has a wavenumber of k_{z_i}, and the $J_m(p_1\rho)$ represents the Bessel function in the ρ -direction in the QD-disk plane These calculations are similar to those in [30].

The momentum matrix element of the WL-QD transition, denoted as μ_{35}, has been explicitly defined, and an assignment for the band's states has been established, particularly during instances in VB. This notation and information are derived from reference [35].

$$\mu_{35} = \langle\varphi_{QD}^{j=3}|e\vec{r}|\varphi_{WLv}\rangle \quad (13)$$

$$\mu_{35} = \langle\psi_{QD}^{j=3}|e\hat{\rho}\rho|\psi_{WLv}\rangle A_{QD_{z3}}A_{w_{z5}}\int\cos(k_{z_v}z)\cos(k_{zw_v}z)\,dz \quad (14)$$

Where $\varphi_{QD}^{j=3}$, φ_{WLv} are the QD state's total wave functions |3⟩ and WL VB, while $\psi_{QD}^{j=3}$ and ψ_{WLv} are those in the ρ-direction. $A_{QD_{z3}}$ and $A_{w_{z5}}$ are the normalization constants of the wave functions in the z-direction.

$$\langle\varphi_{QD}^{j=3}|e\hat{\rho}\rho|\psi_{WLv}\rangle = \frac{1}{N_{WL}}[\langle\varphi_{QD}^{j=3}|e\rho|\psi_{WLv}\rangle -$$

$$\sum_{i=0}^{3}\langle\varphi_{QD}^{j=3}|e\rho|\varphi_{QD}^{i}\rangle\langle\varphi_{QD}^{i}|\varphi_{WLv}\rangle \quad (15)$$

In the OPW in eq. (15), the normalization constant $N_{WL,j}$ is defined by [34],

$$N_{WL}=\sqrt{1-\left|\sum_i\langle\varphi_{QD}^{i}|\varphi_{WL}\rangle\right|^2} \quad (16)$$

Every DQD sub band is included in the summing.

$$\langle\varphi_{QD}^{j=3}|e\rho|\psi_{WLv}\rangle=\frac{C_{mn}|e|}{\sqrt{A}}\int J_{m,j}(p\rho)e^{ik\rho}\rho^2\,d\rho \quad (17)$$

$$\langle\varphi_{QD}^{j=3}|e\rho|\varphi_{QD}^{i=2}\rangle=C_{mn,j}C_{mn,i}|e|\int_0^{h/2}J_{m,j}\,\rho J_{m,i}\rho d\rho \quad (18)$$

$$\langle\varphi_{QD}^{i}|\varphi_{WLv}\rangle=\frac{C_{mn}}{\sqrt{A}}\int J_{m,j}(p\rho)e^{ik\rho}\rho^2 d\rho \quad (19)$$

Then,considering μ_{14} as an illustration of CB's WL-QD transition. It is written as:

$$\mu_{14}=\langle\varphi_{QD}^{j=1}|er|\varphi_{WLc}\rangle \quad (20)$$

$$\mu_{14}=\langle\varphi_{QD}^{j=1}|e\hat{\rho}\rho|\psi_{WLc}\rangle A_{QD_{z1}}A_{w_{z4}}$$

$$\int\cos(k_{z_cz})\cos(k_{zw_cz})\,dz \quad (21)$$

$$\langle\varphi_{QD}^{j=1}|e\hat{\rho}\rho|\psi_{WLv}\rangle=\frac{1}{N_{WL,j}}[\langle\varphi_{QD}^{j=1}|e\rho|\psi_{WLv}\rangle-$$
$$\sum_{i=0}^{1}\langle\varphi_{QD}^{j=1}|e\rho|\varphi_{QD}^{i=0}\rangle\langle\varphi_{QD}^{i=0}|\varphi_{WLc}\rangle \quad (22)$$

With

$$\langle\varphi_{QD}^{j=1}|e\rho|\varphi_{QD}^{i=0}\rangle=C_{mn,j}C_{mn,i}|e|\int_0^{h/2}J_{m,j}\,\rho J_{m,i}\rho d\rho \quad (23)$$

$$\langle\varphi_{QD}^{i=0}|\varphi_{WLc}\rangle=\frac{C_{mn}}{\sqrt{A}}\int J_{m,j}(p\rho)e^{ik\rho}\rho d\rho \quad (24)$$

F. The Susceptibility of DQD-MNP hybrid

Energy scheme of the hybrid DQD-MNP structure is shown in Fig.2. Beside DQD states, We Examined a hybrid DQD - MNP structure where both probe and pump fields presented. The interband transition $|0\rangle\rightarrow|2\rangle$, is driven by a weak probe field E_{02}^0 with Rabi frequency $\Omega_{02}^0=\frac{E_{02}^0\mu_{02}}{2\hbar\varepsilon_{effs}}$. The interband transition $|1\rangle\leftrightarrow|3\rangle$ was due to the pump field E_{13}^0, The controlling field's Rabi frequency can be expressed as $\Omega_{13}^0=\frac{E_{13}^0\mu_{13}}{2\hbar\varepsilon_{effs}}$. For the standing-wave trigger field with Rabi frequency $\Omega_{13}^0\,sin\left(\frac{\pi x}{\Lambda}\right)$ where the standing wave's spatial frequency represented by Λ, and gratings were used to modify the transmission function in the x-direction.

The Rabi frequency of the total electric field is related to the direct coupling of the applied field of the DQD and the induced internal field from the MNP [35,36].

From eq. (9), we wrote the probe Ω_{02} field's effective Rabi frequency,

$$\Omega_{02}=\Omega_{02}^0\left(1+\frac{\gamma_M a^3\delta_\alpha}{R^3}\right) \quad (25)$$

The effective Rabi frequency for the standing-wave trigger field can be written as,

$$\Omega_{13}=\Omega_{13}^0\left(sin\left(\frac{\pi x}{\Lambda}\right)+\frac{\gamma_M a^3\delta_\alpha}{R^3}\right) \quad (26)$$

Using Eq. (25), and Eq.(26) to calculate density matrix Eqs. (11), Under the Standing-Wave field, the linear susceptibility of the probe field represented as:

$$\chi^{(1)}=\frac{2N_Q\mu_{02}}{\varepsilon_0 E_{DQD,02}} \quad (27)$$

Where $N_Q(=\frac{\Gamma}{\pi\rho^2 h_d})$ is the number of DQDs per unit volume, h_d is the QD height, and ε_0 is the vacuum's dielectric constant.

III. RESULTS AND DISCUSSION

The results of the hybrid DQD - MNP system were examined in this section. Other works use selected values for QD energy sub bands and experimental transition momenta, making it easy to obtain results. In this work, we studied the characteristics of materials by calculating QD energy sub bands and subsequently transition momentum to produce outcomes for every structure with its starting set of parameters. Due to the orthogonal zed plane wave (OPW), the quasi-continuum state of the WL effect on the QD transitions was observed.[31, 37]. The results of these calculations were represented in the figure of merit for this work. MAOUD-37 (our lab software), was developed and used in this investigation. It was reported in previous experimental works [38] that addressed various optical qualities [31, 32, 37, and 39]. Plasmatic nanostructures are the subject of some of them [40–42]. Table 1 contains a list of the parameters that were used in our calculations. To facilitate the interpretation of the findings in this work, Table 1 lists the computed QD energy sub bands and the transition moments.

Accordingly, this software begins with the calculation of QD energy levels. Second, the study of transition momenta using Eqs. (12)-(24) were required for the effective Rabi frequencies Ω_{ij} and G_{ij}. The density operator ρ_{02} that was used in the susceptibility calculation was obtained through the numerical solution of the density matrix Eqs. (11). Then, the susceptibility under the Standing-Wave field was calculated. From there, the susceptibility under the Standing-Wave field was computed. It was assumed that the background dielectric constant is $\varepsilon_B=\varepsilon_0$. For simplicity, the relaxation times $(\gamma_0=\gamma_1=\gamma_2=\gamma_3=\gamma_4=\gamma_5)$ for the DQD were taken to be the same [43, 44].The MNP dielectric constant ε_M of the Au bulk dielectric constant [45].We referred for (R and a) values in the figures, i.e., $(R>a>\rho_1,\rho_2)$[14,17].

Table 1: parameters that were used in our calculations:

Parameters	**Values (unit)**	**Ref.**	
$\gamma_0 = \gamma_1 = \gamma_2 = \gamma_3 = \gamma_4 = \gamma_5$	1/(2.5 ns)	[43, 44]	
Γ	6×10^{-3}	[45]	
ε_s	$15.15\varepsilon_0$	[27]	
ε_M	$6.9\varepsilon_0$	[46]	
Momentum	**Values (nm.e)**	**Momentum**	**Values (nm.e)**
μ_{10}	2.5716	μ_{25}	0.0176
μ_{20}	0.0069	μ_{35}	0.0278
μ_{30}	0.0071	μ_{14}	0.0367
μ_{32}	2.3849	μ_{04}	0.0341
μ_{31}	0.0076	μ_{21}	0.0066
QD CB subband	**Values (eV)**	**QD VB subband**	**Values (eV)**
E_{c0}	0.9626	E_{v2}	-0.3555
E_{c1}	1.0288	E_{v3}	-0.3727

Fig. 3 shows the DQD-MNP susceptibility, where a wide radius gave us a high susceptibility. The curve was minimum a few-shifted from a grating period with an increasing MNP radius, while the peak was still at the same point.

Fig. 4 shows the susceptibility at different distances (R) between the centers of the DQD and MNP with a=10nm, $\Omega_{02}^0 = 0.009$ eV , $\Omega_{13}^0 = 18$ GeV, $T_{01} = 0.01\gamma_0, T_{32} = 8\gamma_0$. A high susceptibility is associated with a small R.

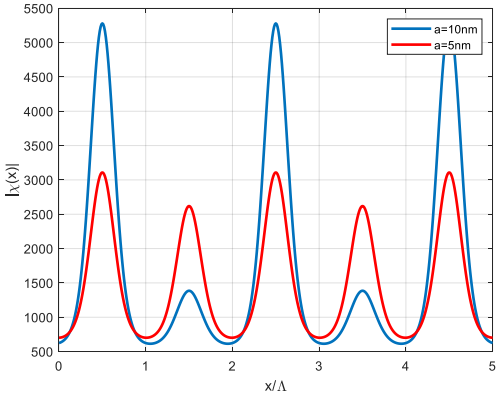

Fig. 3: The DQD-MNP susceptibility at $a = 5, 10\ nm$ MNP radius R=20nm, $\Omega_{02}^0 = 0.009\ eV$, $\Omega_{13}^0 = 18\ GeV, T_{01} = 0.01\gamma_0$,and $T_{32} = 8\gamma_0$.

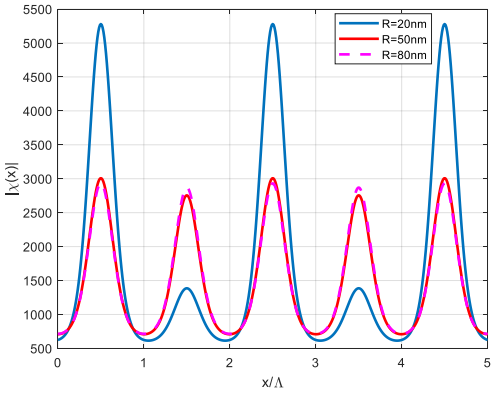

Fig. 4: The DQD-MNP susceptibility at a = 10 nm MNP at different radii R=20, 50, 80nm, $\Omega_{02}^0 = 0.009$ eV, $\Omega_{13}^0 = 18$ GeV, $T_{01} = 0.01\gamma_0$,and $T_{32} = 8\gamma_0$.

Fig. 5 shows susceptibility in the case of including/neglecting metal contribution. using the metal increased the susceptibility, and that explained the reasone of using MNP with QD structures.

Fig.6comparing DQD-MN and single QD (SQD)-MNP susceptibility. This also shows the reason for using DQD instead of QD structures. This comes from the flexibility in the DQD transitions, which can strengthen some transitions.

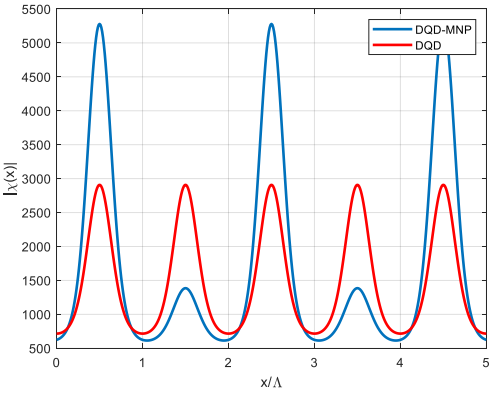

Fig. 5 The DQD-MNP susceptibility at a = 10 nm, MNP radius R=20nm, $\Omega_{02}^0 = 0.009$ eV, $\Omega_{13}^0 = 18$ GeV, $T_{01} = 0.01\gamma_0$, and $T_{32} = 8\gamma_0$.

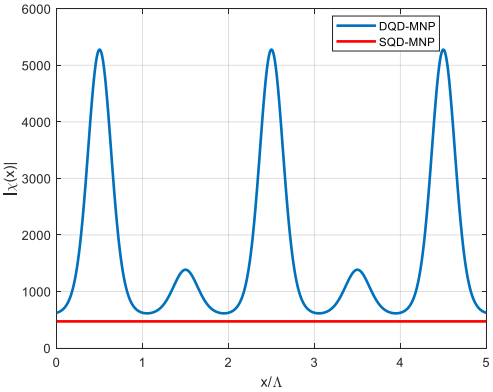

Fig. 6 The DQD-MNP susceptibility at a = 10 nm MNP radius R=20nm, $\Omega_{02}^0 = 0.009$ eV, $\Omega_{13}^0 = 18$ GeV, $T_{01} = 0.01\gamma_0$, and $T_{32} = 8\gamma_0$.

Fig. 7 shows the DQD-MNP susceptibility under different pumpings. The susceptibility reduced with the pump field.

Fig. 8 shows the DQD-MNP susceptibility for different Ω_{02}^{0}.

Fig. 9 shows DQD-MNP susceptibility for different DQD sizes for quantum disk and radius. The smaller size gave us high susceptibility because of the quantization effect.

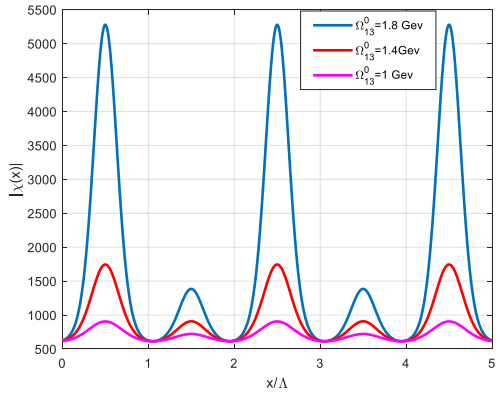

Fig. 7 The DQD-MNP susceptibility at $a = 10$ nm MNP radius R=20nm, $\Omega_{02}^{0} = 0.009$ eV , $T_{01} = 0.01\gamma_0$, and $T_{32} = 8\gamma_0$ at different pumpings.

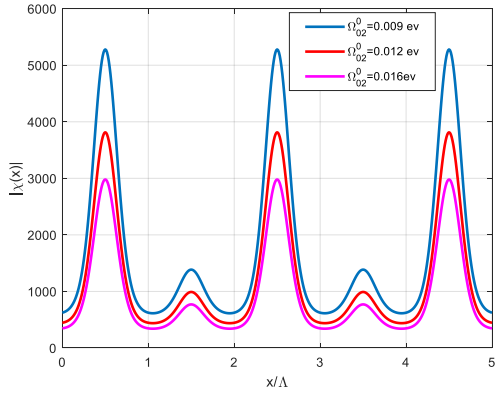

Fig. 8 The DQD-MNP susceptibility at $a = 10$ nm MNP radius R=20nm, $\Omega_{02}^{0} = 0.009$ eV , $\Omega_{13}^{0} = 18$ GeV, $T_{01} = 0.01\gamma_0$, and $T_{32} = 8\gamma_0$ at different probs.

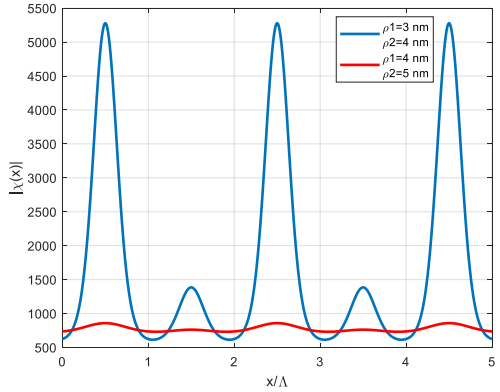

Fig. 9 The DQD-MNP susceptibility at $a = 10$ nm MNP radius R=20nm, $\Omega_{02}^{0} = 0.009$ eV, $\Omega_{13}^{0} = 18$ GeV, $T_{01} = 0.01\gamma_0$, and $T_{32} = 8\gamma_0$.

Fig. 10 shows DQD-MNP susceptibility at different values of the tunneling component T_01. An interesting result is shown in the inverting of the grating period with tunneling.

Fig. 11 shows the DQD-MNP susceptibility at various tunneling component T_23 values. This component only reduces the susceptibility.

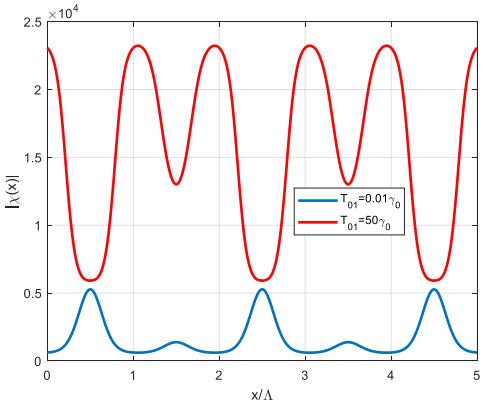

Fig. 10 The DQD-MNP susceptibility at $a = 10$ nm MNP radius R=20nm, $\Omega_{02}^{0} = 0.009$ eV, $\Omega_{13}^{0} = 18$ GeV, $T_{32} = 8\gamma_0$, and different tunnelings.

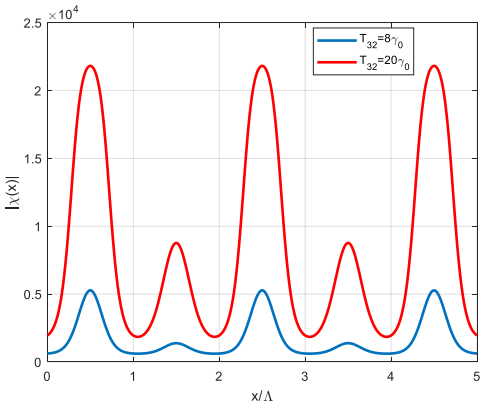

Fig. 11 The DQD-MNP susceptibility at $a = 10$ nm MNP radius R=20nm, $\Omega_{02}^{0} = 0.009$ eV , $\Omega_{13}^{0} = 18$ GeV, $T_{01} = 0.01\gamma_0$, and different tunnelings.

IV. Conclusions

In this work, the application of the standing wave field of the orthogonalized plane wave (OPW) between each DQD and WL-QD transition, as well as the impact of WL, were calculated, The susceptibility is reduced with decreasing the pump field under a standing-wave field. Using MNP with QD structures in the presence of metal increased the susceptibility. Moreover, the pump field reduced the susceptibility. Finally, an interesting result was shown in the inverting of the grating period with the tunneling component in the conduction band.

CONFLICT OF INTEREST

Authors declare that they have no conflict of interest.

References

[1] M.-T. Cheng, S.-D. Liu, H.-J. Zhou, Z.-H. Hao, and Q.-Q. Wang, "Coherent exciton-plasmon interaction in the hybrid semiconductor quantum dot and metal

nanoparticle complex,"*Opt. Lett*., vol. 32, no. 15, pp. 2125, 2007.

[2] S. M. Sadeghi, "The inhibition of optical excitations and enhancement of Rabi flopping in hybrid quantum dot-metallic nanoparticle systems," *Nanotechnology*, vol. 20, no. 22, pp. 20–26, 2009.

[3] A. Smponias, D. Stefanatos, and E. Paspalakis, "Fast and robust exciton preparation inacoupled semiconductor quantum dot-metal nanoparticle system using shortcuts to adiabaticity," *J. Appl. Phys.*, vol. 129, pp. 123107, 2021.

[4] A. Smponias, D. Stefanatos, and E. Paspalakis, "Efficient Biexciton State Preparation in a Semiconductor Quantum Dot-Metallic Nanoparticle Hybrid Structure Using Transitionless Quantum Driving," *Ann. Phy.*, vol. 534, pp. 2270001, 2022.

[5] J. Lee, A. O. Govorov, J. Dulka, and N. A. Kotov, Bioconjugates of CdTe nanowires and Au nanoparticles plasmon-exciton interactions, luminescence enhancement, and collective effects, *Nano Lett*., vol.4 pp. 2323–2330, 2004.

[6] K. T. Shimizu, W. K. Woo, B. R. Fisher, H. J. Eisler, and M. G. Bawendi, "Surface-enhanced emission from single semiconductor nanocrystals," *Phys. Rev. Letters*, vol. 89, pp. 117401, 2002.

[7] A. O. Govorov and H. H. Richardson, "Generating heat with metal nanoparticles," *Nano Today*, vol. 2, pp. 30–38, 2007.

[8] S. M. Sadeghi, "Coherent control of metallic nanoparticles near fields: Nanopulse controllers and functional nanoamplifiers," *Phys. Rev. B*, vol. 82, pp. 1-7, 2010.

[9] A. Ridolfo, O. Di Stefano, N. Fina, R. Saija, and S. Savasta, "Quantum plasmonics with quantum dot-metal nanoparticle molecules: Influence of the fano effect on photon statistics," *Phys. Rev. Lett*., vol. 105, no. 26, pp. 263601, 2010.

[10] Z. Lu and K. Di Zhu, "Slow light in an artificial hybrid nanocrystal complex," *J. Phys. B At. Mol. Opt. Phys*., vol. 42, no. 1, pp. 015502, 2009.

[11] E. Paspalakis, S. Evangelou, and A. F. Terzis, "Control of excitonic population inversion in a coupled semiconductor quantum dot-metal nanoparticle system," *Phys. Rev. B*, vol. 87, no. 23, pp. 235302, 2013.

[12] S. M. Sadeghi, "Gain without inversion in hybrid quantum dot-metallic nanoparticle systems," *Nanotechnology*, vol. 21, no. 45, pp. 455401, 2010.

[13] H. Xu, J. Liu, X. Duan, J. Li, J. Xue, X. Sun, Y. Cai, Z. Zhou, and X. Wang, Enhance energy transfer between quantum dots by the surface plasmon of Ag island film, *Opt. Mater. Express*, vol. 4, PP. 2586-2594, 2014.

[14] A. V. Malyshev and V. A. Malyshev, "Optical bistability and hysteresis of a hybrid metal-semiconductor nanodimer," *Phys. Rev. B - Condens. Matter Mater. Phys*., vol. 84, no. 3, pp. 035314, 2011.

[15] . G. Kosionis and E. Paspalakis, "Pump-probe optical response of semiconductor quantum dot—Metal nanoparticle hybrids," *J. Appl. Phys*., vol. 124, pp. 223104, 2018.

[16] Y. Zhao and Y. Jiang, "Effect of KrF excimer laser irradiation on the properties of ZnO thin films," *J. Appl. Phys.*, vol. 103, no. 11, pp. 114903, 2008.

[17] J. H. Huang and R. Chang, "Nonlocal and nonlinear effects on the dispersion relation for surface plasmon at a metal-Kerr medium interface," *J. opt.*, vol. 12, pp. 045003, 2010.

[18] X. N. Liu, D. Z. Yao, H. M. Zhou, F. Chen, and G. G. Xiong, Third-order nonlinear optical response in quantum dot-metal nanoparticle hybrid structures, *Appl. Phys. B*, vol. 113, pp.603-610, 2013.

[19] A. F. Terzis, S. G. Kosionis, J. Boviatsis, and E. Paspalakis, Nonlinear optical susceptibilities of semiconductor quantum dot—Metal nanoparticle hybrids, *J. Mod. Opt.*, vol. 63, pp. 451-461, 2016.

[20] S. Evangelou, V. Yannopapas, and E. Paspalakis, "Modification of Kerr nonlinearity in a four-level quantum system near a plasmonic nanostructure," J. *mod. opt*., vol. 61, pp. 1458-1464, 2014.

[21] J.-B. Li, M.-D. He, and L.-Q. Chen, "Four-wave parametric amplification in semiconductor quantum dot-metallic nanoparticle hybrid molecules," *Opt. Express*, vol. 22, no. 20, p. 24734, 2014.

[22] V . V. Flambaum and V. A. Dzuba, "Electric dipole moments of atoms and molecules produced by enhanced nuclear Schiff moments," *Phys. Rev. A*, vol. 101, pp. 1-12, 2019.

[23] M. R. Avadi, A. M. Sadeghi, N. Mohammadpour, S. Abedin, F. Atyabi, R. Dinarvand, M. Rafiee-Tehrani, "Preparation and characterization of insulin nanoparticles using chitosan and Arabic gum with ionic gelation method," *Nanomedicine*, vol. 6, pp. 58-63, 2010.

[24] E. Paspalakis, S. Evangelou, S. G. Kosionis, and A. F. Terzis, "Strongly modified four-wave mixing in a coupled semiconductor quantum dot-metal nanoparticle system," *J. Appl. Phys.*, vol. 115, pp. 083106, 2014.

[25] S. K. Singh, M. K. Abak, and M. E. Tasgin, "Enhancement of four-wave mixing via interference of multiple plasmonic conversion paths," *Phys. Rev. B*, vol. 93, pp. 035410, 2016.

[26] S. G. Kosionis, E. Paspalakis, "Absorption and Dispersion Properties of a Coupled Asymmetric Double Quantum Dot Molecule–Metal Nanoparticle Structure," *Engineering Proceedings*, vol. 56, no.1, pp. 244, 2023.

[27] S. L.Chuang, Physics of optoelectronic devices, 1st Edition, Wiley, New Jersy, (1995).

[28] R. D. Artuso and G. W. Bryant, "Optical response of strongly coupled quantum dot-metal nanoparticle systems: Double peaked Fano structure and bistability," *Nano Letters*, vol. 8, no. 7, pp. 2106–2111, 2008.

[29] R. D. Artuso and G. W. Bryant, Strongly coupled quantum dot-metal nanoparticle systems: Exciton-induced transparency, discontinuous response, and suppression as driven quantum oscillator effects, *Phys. Rev. B*, vol. 82, pp. 195419, 2010.

[30] A. Yariv, Quantum Electronics, Wiley, New York, (1975).

[31] H. G. Al-Toki and A. H. Al-Khursan, "Negative refraction in the double quantum dot system," *Opt. Quantum Electron*, vol. 52, pp. 467, 2020.

[32] H. Akram and A. H. Al-Khursan, "Second-order nonlinearity in ladder plus-Y configuration in double quantum dot structure," *Appl. Opt.*, vol. 55, pp. 9866-9874, 2016.
[33] A. H. Flayyih, and A. H. Al-Khursan, "Integral gain in quantum dot semiconductor optical amplifiers," *Superlattices and Microstructures*, vol. 62, pp. 81-87, 2013.
[34] E. Rehman and A. H. Al-Khursan, "All-optical processes in double quantum dot structure," *Appl. Opt*., vol. 55, pp. 7337-7344, 2016.
[35] E. Placidi, F. Arciprete, V. Sessi, M. Fanfoni, F. Patella, and A. Balzarotti," Step erosion during nucleation of InAs ⁄ GaAs (001) quantum dots," *Applied Physics Letters*, vol. 86, no. 24, pp. 241913, 2005.
[36] M. Markiewicz, H. Voss, "Electronic States in Three Dimensional Quantum Dot/Wetting Layer Structures", *Lecture Notes in Computer Science*, vol. 3980, pp. 684–693, 2006.
[37] H. H. Al-Ameri, M. Abdullah, and A. H. Al-Khursan, "Entanglement in ladder-plus-Y-double quantum dot structure via entropy," *Appl. Opt.*, vol. 58, pp. 369-382, 2019.
[38] F. R. Al-Salihi and A. H. Al-Khursan, "Electromagnetically induced grating in double quantum dot system using spontaneously generated coherence," *Chin. J. Phys*., vol. 70, pp. 140-150, 2021.
[39] J. N. Jabir, S. M. M. Ameen, and A. H. Al-Khursan, "Plasmonic quantum dot nanolaser: Effect of ‘waveguide Fermi energy," *Plasmonics*, vol. 14, pp. 1881-1891, 2019.
[40] J. N. Jabir, S. M. M. Ameen, and A. H. Al-Khursan, "Plasmonic quantum dot nanocavity laser: Hybrid modes," *Plasmonics*, vol. 15, pp. 1451-1458, 2020.
[41] J. N. Jabir, S. M. M. Ameen, and A. H. Al-Khursan, "Modeling of dielectric function in plasmonic quantum dot nanolaser," *Opt. Quantum Electron*, vol. 51, pp. 396, 2019.
[42] M. Gioannini and I. Montrosset, "Numerical Analysis of the Frequency Chirp in Quantum-Dot Semiconductor Lasers," *IEEE J. Quantum Electronics*, vol. 43, pp. 941-949, 2007.
[43] S. Hadi and A. H. Al-Khursan, "Recombination rates of the double quantum dot solar cell structure," *Phys. Scr*., vol. 96, pp. 125820, 2021.
[44] C. H. Yuan and K. Di Zhu, "Voltage-controlled slow light in asymmetry double quantum dots," *Appl. Phys. Lett*., vol. 89, pp. 1-4, 2006.
[45] I. N. Shklyarevskii and P. L. Pakhmov, "Optoelectronic Properties Correlation to Preparation of Au/La-oxide Nanocomposite Films," *Science of Sintering*, vol. 45, pp. 189-197, 2013.
[46] J. Y. Yan, W. Zhang, S. Duan, X. G. Zhao, and A. O. Govorov, "Optical properties of coupled metal-semiconductor and metal-molecule nanocrystal complexes: Role of multipole effects," *Phys. Rev*., vol. 77, no. 16, pp. 165301, 2008.